Multicenter continuum distorted wave with eikonal initial state model for single ionization in ion-molecule collisions: Differential electron emission from water under energetic ion impact

L. Gulyás
Institute for Nuclear Research (ATOMKI), 4026 Debrecen Bem Tér 18/C, H-4026 Debrecen, Hungary

(Received 11 May 2023; accepted 13 September 2023; published 22 September 2023)

A multicenter continuum distorted wave with eikonal initial state model for single ionization of molecules by energetic ion impact is developed. The multicenter nature of the molecular ion is explicitly taken into account, within the framework of the independent electron approach, where the interaction between the ejected electron and the residual molecular ion is described by an anisotropic model potential. The method is employed to calculate doubly and singly differential cross sections of the water molecule by energetic H^+, C^{6+}, and O^{8+} projectiles. The discussion of the results is primarily focused on the emission of low-energy electrons, where the evaluated cross sections are compared with experimental and available theoretical data.

DOI: 10.1103/PhysRevA.108.032815

I. INTRODUCTION

Ionization of atoms and molecules by fast charged particles has been the subject of active research in the last few decades [1–4]. A number of experimental and theoretical studies have been devoted to revealing mechanisms responsible for the ejection of one or more electrons [5–9]. The great interest is partially motivated by increasing applications, as plasma physics, ion therapy, and radiation protection. Motivation for understanding the collision governed large-scale processes in space and in planetary atmospheres is also getting stronger [10]. It has been shown for atomic targets that theoretical models formulated within the continuum distorted wave with eikonal initial sate (CDW-EIS) approximation [11] with Hartree-Fock description of bound and continuum electronic orbitals yield very good agreement with experiments [1,12,13]. For molecules, an equivalent scheme for the calculation of scattering quantities is a nontrivial task. The well-known GAUSSIAN program [14], which provides multicenter wave functions, can generally be applied to describe the ground state properties of molecular targets. The central field model, applied to the description of bound and continuum electronic states of atoms, enables the factorization of the wave function in its radial and angular parts [15]. Extension of the model to the multicenter molecular quantities is known as the single-center-expansion (SCE) method [16]. The SCE method extends the application of procedures introduced in the treatment of atomic collisions to the analysis of molecular processes. However, one of the main obstacles to adaptation lies in a precise description of the wave function for the ejected electron that explicitly takes into account the multicenter nature of the recoiling molecular ion. Accounting for the interaction between the ejected electron and the residual molecular ion is a rather complex problem, and the potential field in which the ejected electron moves is often modeled as the sum of the local electrostatic potential, the nonlocal exchange contribution, and the equally non-local polarization-correlation potential [16,17]. Therefore, in the vast majority of applications, in order to reduce the computational task, the interaction between the molecular core and the released electron is approximated by a Coulomb potential with an effective charge corresponding to the ionization energy of the ejected electron [9,18–21]. Obviously, in all of these calculations, the molecular orbitals in the initial and final channels are not orthogonal. The importance of orthogonality, the evaluation of electron orbitals on the same potential both in the entry and exit channels, is well known in the case of atomic collisions [12].

Adaptation of the CDW-EIS method to molecular collisions, where the molecular continuum orbital is described in the multicenter field of the residual molecular ion, was done by Nascimento *et al.* [22]. The molecular orbital in the continuum has been calculated with the Swinger variational iterative method, where the multicenter static-exchange potential acting on the ejected electron has been derived using the ground state density (CDW-EIS-SVIM model). The orthogonality between the initial and final molecular orbitals is ensured. The method has been applied to the single ionization of hydrogen molecule by energetic bare ion impacts. The calculated doubly differential cross section (DDCS) revealed nice agreement with the experiment for all the studied quantities. In the CDW-EIS-SVIM model the ground state molecular orbitals have been expanded over the internuclear center of mass, and application of the method to other more complex molecules is straightforward. However, to the best of our knowledge, application of the model to molecules other than the H_2 molecule is not available in the literature.

In this work, we generalize the CDW-EIS method to molecular collisions and apply it to evaluate DDCSs for the single ionization of H_2O by energetic bare ion impacts. As in our previous application of the method [23], the initial ground state molecular orbitals are described with the GAUSSIAN quantum chemistry program package [14] at the Hartree-Fock level. However, the SCE procedure is used not only for the initial orbitals, but also for the ground state electron density, with which the static and exchange contributions to the

 ©2023 American Physical Society

potential accounting for the multicenter interaction between the unbound electron and the target core are derived. That is compared to our previous application of the CDW-EIS model, where the continuum orbital was evaluated on the spherically averaged static potential [23]; a more realistic anisotropic potential is considered to account for the interaction of the released electron with the residual ion in the present treatment. The nonlocal nature of the exact exchange potential requires the solution of integrodifferential equations. One way to simplify the solution and to reduce the computational task is the use of local exchange potential [24]. The local energy-dependent exchange potential proposed by Hara [25] is applied in the present study, and is able to reproduce the essential characteristics of the interaction between bound electrons and the ejected electron.

About two-thirds of the human body is water, and the recent developments in the field of hadron therapy using protons or fast heavy ions require an increasingly throughout knowledge of mechanisms responsible for the electron ejection [3,8,26–28]. Precise stopping power cross sections for the collisions of ion beam with H_2O molecules are needed to plan therapeutic treatment during a Monte Carlo simulation [29]. Electrons from the direct ionization can cause secondary interaction with the biological medium. It is known that the total yield of electrons are dominated by electrons with low ejection energy. For example, 70–75% of the total electron yield is given by electrons with an energy of less than 40 eV when the impact energy of protons ranges from a few hundred keV to a few MeV. DDCS measurements at low electron energies are extremely difficult due to various influencing factors, such as the Earth's magnetic field, etc. [5,30], and discrepancies between the measured and the calculated data of as much as 50% are not uncommon [21,31]. Therefore, accurate and reliable theoretical knowledge and predictions in this area are of great importance. Furthermore, the anisotropic potential field of the molecule is expected to have a significant effect on the movement of low-energy electrons, which also motivated our present discussion of the DDCS focused on the low electron emission energies. It is worth mentioning the recent advances in the theoretical study of electron molecule collisions under a similar scenario [32–34].

The paper is organized as follow: the generalization of the CDW-EIS model for molecular collisions is described in Sec. II. In Sec. III A DDCS for various bare projectile impacts are presented. Single differential cross sections (SDCSs) and total cross sections (TCSs) are considered in Sec. III B. The conclusion is drawn in Sec. IV. Atomic units are used throughout unless indicated otherwise.

II. THEORY

Let us consider the single ionization of the water molecule by bare X^{q+} ion impact,

$$X^{q+} + H_2O \rightarrow X^{q+} + H_2O^+ + e^-, \tag{1}$$

where the projectile is one of the bare ions H^+, C^{6+}, and O^{8+}. The impact energies considered here are high enough so that the vibrational and rotational periods of the target are much larger than the characteristic time of the collision. It is then possible to assume that the molecular nuclei remain fixed in their initial positions during the reaction. In order to reduce the description of the multiparticle collision to the reaction of three particles, it is supposed that each electron is ionized independently of the other electrons, whose states are considered to be frozen during the collision. The wave function of the ejected electron, in the impact parameter approximation [35], could be obtained by solving the Schrödinger equation defined through the electronic Hamiltonian

$$H_{\rm el} = T_{\rm el} + V_T(\mathbf{x}) + V_P(\mathbf{s}), \tag{2}$$

where $\mathbf{x}$ ($\mathbf{s}$) denotes the position vector of the active electron with respect to the center of mass of the target (projectile). $T_{\rm el}$ is the electron kinetic-energy operator and $V_P(s)$ is the Coulomb interaction of the projectile. $V_T = V_{\rm st} + V_{\rm exc}$, where

$$V_{\rm st}(\mathbf{x}) = \int \rho(\mathbf{r}) \frac{1}{|\mathbf{x}-\mathbf{r}|} d\mathbf{r} - \sum_n \frac{Z_n}{|\mathbf{x}-\mathbf{R}_n|} \tag{3}$$

is the static potential of the core electrons and the nuclei. $\rho(\mathbf{r})$ stands for the one-electron charge density [16,24] and $\mathbf{R}_n$ is the position of the nth nucleus with charge Z_n. $V_{\rm exc}$ is the nonlocal exchange potential. Different models are available to approximate $V_{\rm exc}$ with a local potential [24,36], and here we use the method proposed by Hara [25] based on the free-electron-gas model as

$$V_{\rm exc}(k,\mathbf{x}) = \frac{2}{\pi} k_F(\mathbf{x}) \left(\frac{1}{2} + \frac{1-\eta^2}{4\eta} \ln \left| \frac{1+\eta}{1-\eta} \right| \right), \tag{4}$$

with

$$\eta(\mathbf{x}) = \frac{\sqrt{k^2 + 2I + k_F^2}}{k_F}, \tag{5}$$

where $k_F = [3\pi^2 \rho(\mathbf{x})]^{(1/3)}$ is the Fermi momentum, I is the ionization potential of the molecular ion, and $\mathbf{k} = (k, \theta_k, \varphi_k)$ is the momentum of the ejected electron. Note that V_T due to the spatial arrangement of the nuclei possesses a multicenter nature and has angular distributions, which complicates the description of the process.

Molecular wave functions are more conveniently evaluated in the coordinate system fixed to the molecule [body frame (BF) of reference], where the coordinates are marked with primes. In order to reduce the complexity of the problem, as far as possible, full account is taken of the restrictions imposed on the problem by the symmetry of the molecule. Bearing in mind that a molecule possesses point group symmetry in the molecular frame, the symmetry-adapted angular function $X_{hl}^{p,\mu}(\theta', \varphi')$ would be the prior choice and is employed in this work, where p and μ label one of the relevant irreducible representations and one of its components, respectively [16,37]. Index h labels a specific basis, at a given angular momentum l, for the pth irreducible representations considered. The symmetry-adapted angular function can be transformed from the spherical harmonics with the symmetry-dependent transformation matrix [16,37]

$$X_{hl}^{p\mu}(\hat{\mathbf{x}}') = \sum_m b_{hlm}^{p\mu} Y_l^m(\hat{\mathbf{x}}'). \tag{6}$$

Taking into account the symmetry of the molecule and employing the single-center expansion method, a given $\Phi_i(\mathbf{x}')$

multicenter bound molecular orbital, defined with GAUSSIAN16, can be written as [16]

$$\Phi_i(\mathbf{x}') = \sum_{h_i l_i} u_{h_i l_i}(x') X^{p\mu}_{h_i l_i}(\hat{\mathbf{x}}'), \tag{7}$$

where the coefficients are evaluated as

$$u_{h_i l_i}(x') = \int d\hat{\mathbf{x}}' \left[X^{p\mu}_{h_i l_i}(\hat{\mathbf{x}}')\right]^* \Phi_i(\mathbf{x}'), \tag{8}$$

and $\mathbf{x}'$ refers to the center of mass of the molecule. The potentials (3) and (4) can also be expanded over the symmetry adapted spherical harmonics belonging to the A_1 irreducible representation as

$$V_{\rm sx}(\mathbf{x}') = \sum_{lm} v^{A_1,{\rm sx}}_{lm}(x') X^{A_1}_{lm}(\mathbf{x}'), \tag{9}$$

where sx refers to st or exc.

The continuum orbital of the ejected electron is obtained with the partial-wave-expansion method as

$$\Phi_{\mathbf{k}'}(\mathbf{x}') = \frac{1}{x\sqrt{k'}} \sum_{p\mu} \sum_{hl} \sum_{h'l'} i^l e^{-i\delta_l} u_{h'l',hl}(k', x') \times [X^{p\mu}_{h'l'}(\hat{\mathbf{x}}')] X^{p\mu}_{hl}(\hat{\mathbf{k}}') \tag{10}$$

where $u_{h'l',hl}(k', x')$ is the solution of the radial equation

$$\left[\frac{d^2}{dx'^2} - \frac{l'(l'+1)}{x'^2} + k'^2\right] u_{h'l',hl}(k', x') = 2 \sum_{h''l''} V^{p\mu}_{h'l',l''h''}(k', x') u_{h''l'',hl}(k', x'), \tag{11}$$

where the potential matrix elements is given by

$$V^{p\mu}_{h'l',h''l''}(k', x') = \left\langle X^{p\mu}_{h'l'}(\hat{\mathbf{x}}') \middle| V_{\rm st}(\mathbf{x}') + V_{\rm exc}(k', \mathbf{x}') \middle| X^{p\mu}_{h''l''}(\hat{\mathbf{x}}') \right\rangle. \tag{12}$$

Equation (11) is solved numerically, where the asymptotic solutions are constructed satisfying the real K matrix boundary conditions [38]

$$u_{h'l',hl}(k', x') \xrightarrow{x'\to\infty} \sqrt{\frac{2}{\pi k}} [\sin(\theta_{h'l'} + \delta^c)\delta_{hh'}\delta_{ll'} + \cos(\theta_{h'l'} + \delta^c) K_{hl,h'l'}], \tag{13}$$

where $\theta_{hl} = k'x' - l\pi/2 - \eta \ln(2k'x')$, with $\eta = 1/k'$ and δ^c is the Coulomb phase shift.

The above description of the wave functions are given in the molecular BF of reference. However, the scattering quantities are evaluated in the laboratory frame (LF) of reference. Therefore, we need to transform the BF expressions of the orbitals into the LF one, where the coordinates are without prime. The molecular orientation is defined by the Euler angles $\omega_E = (\alpha, \beta, \gamma)$, and the molecular wave function in the laboratory frame can be obtained by applying the transformation properties of the spherical harmonics

$$Y_{lv}(\hat{\mathbf{x}}) = \sum_{m'} D^l_{m'v}(\Omega) Y_{lm'}(\hat{\mathbf{x}}') \tag{14}$$

and the symmetry adapted spherical harmonics

$$X^{p\mu}_{lh}(\hat{\mathbf{x}}) = \sum_{m'} \bar{b}^{p\mu}_{l'h'm'} D^l_{m'v}(\Omega) Y_{lm'}(\hat{\mathbf{x}}'), \tag{15}$$

where $\bar{b}$ denotes the appropriate expansion coefficient [16,37].

Considering the single center expansion of the molecular orbitals and their transformation properties to the LF frame of reference, we are now able to describe the dynamics of the collision within the frame of the CDW-EIS model as derived previously for atomic systems [12]. The effect of the projectile on the electronic orbital is taken into account by using eikonal distorted wave function

$$\xi^+_{i,\omega_E}(\mathbf{x}, t) = e^{-i\varepsilon_i t} \Phi_{i,\omega_E}(\mathbf{x}) E^*_{\mathbf{v}}(\mathbf{s}, \eta_i) \tag{16}$$

for the initial channel, and by the Coulomb distorted wave function

$$\xi^-_{\mathbf{k},\omega_E}(\mathbf{x}, t) = e^{-i\varepsilon_k t} \Phi^-_{\mathbf{k},\omega_E}(\mathbf{x}) D_{\mathbf{p}}(\mathbf{s}, \eta_P) \tag{17}$$

for the ionization channel. The distortion factors $D_{\mathbf{p}}(\mathbf{s}, \eta_P)$ and $E^*_{\mathbf{v}}(\mathbf{s}, \eta_i)$ are given by

$$D_{\mathbf{p}}(\mathbf{s}, \eta_p) = e^{\pi\eta_p/2}\Gamma(1 + i\eta_p)\,{}_1F_1(-i\eta_p, 1, -i(ps + \mathbf{p}\cdot\mathbf{s})) \tag{18}$$

and

$$E_{\mathbf{v}}(\mathbf{s}, \eta_i) = (vs + \mathbf{v}\cdot\mathbf{s})^{i\eta_i}, \tag{19}$$

respectively, where $\eta_i = Z_P/v$, $\eta_P = Z_P/p$, $\mathbf{p} = \mathbf{k} - \mathbf{v}$, $\mathbf{s} = \mathbf{x} - \mathbf{R}$, and ${}_1F_1$ is the confluent hypergeometric function. ω_E reflects the fact that the orbitals were originally derived in the BF frame and transformed to SF frame of reference; see Eqs. (7), (10), (14) and (15).

The transition amplitude as a function of impact parameter $\boldsymbol{\rho}$, in the *prior* form of CDW-EIS, can be written as [11,39]

$$a^-_{i\mathbf{k}}(\boldsymbol{\rho}, \omega_E) = -\mathrm{i}\int_{-\infty}^{\infty} dt \left\langle \xi^-_{\mathbf{k}\omega_E}(\mathbf{x}, t) \middle| \left(H_{\rm el}(\mathbf{x}, t) - \mathrm{i}\frac{\partial}{\partial t}\right) \xi^+_{i\omega_E}(\mathbf{x}, t) \right\rangle, \tag{20}$$

where

$$\left(H_{\rm el}(\mathbf{x}, t) - i\frac{\partial}{\partial t}\right) \xi^+_{i,\omega_E}(\mathbf{x}, t) = -e^{-i\varepsilon_i t} \left[\Phi_{i,\omega_E}(\mathbf{x}) \frac{1}{2} \nabla^2_{\mathbf{x}} E^*_{\mathbf{v}}(\mathbf{s}, \eta_i) + \nabla_{\mathbf{x}} \Phi_{i,\omega_E}(\mathbf{x}) \cdot \nabla_{\mathbf{s}} E^*_{\mathbf{v}}(\mathbf{s}, \eta_i)\right]. \tag{21}$$

In the impact parameter model it is more convenient to evaluate the transition amplitude as a function of the transverse momentum transfer ($\boldsymbol{\eta}$) as

$$R_{if}(\boldsymbol{\eta}, \omega_E) = \frac{1}{2\pi} \int d\boldsymbol{\rho} \exp(i\boldsymbol{\eta}\boldsymbol{\rho}) a_{if}(\boldsymbol{\rho}, \omega_E). \tag{22}$$

For a given ith initial orbital that belongs to the μ_ith irreducible representation, taking into account Eq. (15), the transformation of the BF orbitals [Eqs. (7) and (10)] to the SF orbitals, $R_{if}(\boldsymbol{\eta}, \omega_E)$, can be written as

$$R_{if}(\boldsymbol{\eta}, \omega_E) = \sum_{p\mu} \sum_{l_i h_i \nu_i} \sum_{l'h'\nu'} \sum_{lh\nu} \bar{b}^{p_i\mu_i}_{l_i h_i \nu_i} \bar{b}^{p\mu}_{l'h'\nu'} \bar{b}^{p\mu}_{lh\nu} D^{l_i}_{\nu_i m_i}(\omega_E) \times D^{l'}_{\nu' m'}(\omega_E) D^{l}_{\nu m}(\omega_E) R^{l_i m_i l' m' l m}_{if}(\boldsymbol{\eta}). \quad (23)$$

The formulation and the expression of $R^{l_i m_i l' m' l m}_{if}(\boldsymbol{\eta})$ is similar to that presented in [12] for the case of an atomic target when the principal and angular quantum numbers of atomic orbitals are related to those appearing in the expressions of $\Phi_{i,\omega_E}(\mathbf{x})$ and $\Phi_{\mathbf{k},\omega_E}(\mathbf{x})$.

The double differential cross section for ejection of an electron with energy ϵ $(= 1/k^2)$ into solid angle $\Omega_k = [\sin(\theta_k) d\theta_k d\varphi_k]$ can be written as

$$\frac{d^2\sigma}{d\epsilon\, d\Omega_k d\omega_E} = \int d\boldsymbol{\eta} |R_{if}(\boldsymbol{\eta}, \omega_E)|^2. \quad (24)$$

The molecules have an arbitrary orientation in the experiments that will be discussed in the next section, therefore we average the cross sections in Eq. (24) over the Euler angles,

$$\frac{d^2\sigma}{d\varepsilon\, d\Omega_k} = \frac{1}{8\pi^2} \int d\omega_E \frac{d^2\sigma}{d\varepsilon\, d\Omega_k d\omega_E}, \quad (25)$$

where the integral over ω_E ($\int d\omega_E = \int_0^{2\pi} d\alpha \int_0^{\pi} d\beta \sin\beta \int_0^{2\pi} d\gamma$) is analytic owing to the orthogonal properties of the $D^m_{l,\mu}$ functions [40]. We take advantage of the addition theorem of the Wigner D functions and write the amplitude in the j_t angular momentum transfer basis [41],

$$\frac{d^2\sigma}{d\varepsilon\, d\Omega_k} = \sum_{j_t m_t n_t} \int d\, d\boldsymbol{\eta} \left| d^{j_t}_{m_t n_t}(\boldsymbol{\eta}) \right|^2, \quad (26)$$

where

$$d^{j_t}_{m_t n_t}(\boldsymbol{\eta}) = \sum_{p\mu} \sum_{l_i h_i \nu_i} \sum_{l'h'\nu'} \sum_{lh\nu} \sum_{j_1 m_1 n_1} \bar{b}^{p_i\mu_i}_{l_i h_i \nu_i} \bar{b}^{p\mu}_{l'h'\nu'} \bar{b}^{p\mu}_{lhm} (-1)^{m'-|\nu'|+m_1-n_1+m_t-n_t} \times \begin{pmatrix} l' & l & j_1 \\ -m' & m & m_1 \end{pmatrix} \begin{pmatrix} j_1 & l_i & j_t \\ -m_1 & m_i & m_t \end{pmatrix} \begin{pmatrix} l' & l & j_1 \\ -|\nu_1| & |\nu_2| & n_1 \end{pmatrix} \begin{pmatrix} j_1 & l_i & j_t \\ -n_1 & |\nu_i| & n_t \end{pmatrix} \times R^{l_i m_i l' m' l m}_{if}(\boldsymbol{\eta}). \quad (27)$$

Single differential and total ionization cross sections are obtained as

$$\frac{d\sigma}{d\varepsilon} = \int d\Omega_k \frac{d^2\sigma}{d\varepsilon d\Omega_k}, \quad (28)$$

$$\frac{d\sigma}{d\Omega_k} = \int d\varepsilon \frac{d^2\sigma}{d\varepsilon d\Omega_k}, \quad (29)$$

$$\sigma = \int d\varepsilon \frac{d^2\sigma}{d\varepsilon}, \quad (30)$$

The symmetry of the H_2O molecule is represented by the C_{2v} point group having the A_1, A_2, B_1, and B_2 irreducible representations, and the ground state of the molecule is described by the $(1a_1)^2(2a_1)^2(1b_2)^2(3a_1)^2(1b_1)^2$ configuration [42,43]. In the present calculations, all the bound molecular orbitals are evaluated within the Hartree-Fock level using the 6-311G basis sets provided by the GAUSSIAN16 program package [44]. The $2a_1$, $1b_2$, $3a_1$, $1b_1$ orbitals were found to give the dominant contributions to the evaluated cross sections. In the SCE description of the initial orbitals [see Eq. (7)], the partial waves up to the angular momentum $l_i = 4$–5 were found to be sufficient to the get convergent DDCS values in (24). The radial functions $u^{p\mu}_{hl,h'l'}$ are determined by numerical integration of (11) with the Numerov algorithm. The number of partial wave expansion terms in the continuum wave function required to achieve the convergence in the DDCS calculation depends on the energy of electrons. The maximum values of l ($l_{\max}$) were set to 5, 8, and 15, respectively, for electron energies of $\epsilon = 2$, 10, and 40 eV. The computation time increases significantly with the increase of $l_{\max}$. For $\epsilon = 2$ eV the DDCS, at a given emission angle, can be determined in about 40 minutes, which increases by 4–5 times at $\epsilon =$ 30 eV on a single node of a 2.4 GHz PC class workstation. At electron energies greater than $\epsilon = 40$ eV, as will be shown below, calculations with spherically averaged potentials give realistic DDCS results. In our previous study for the ionization of H_2O, the wave functions of the ejected electrons were evaluated on a screened Coulomb potential, the spherically averaged potential of the H_2O^+ ion [23]. The spherically averaged potential is the $v^{A_1,\mathrm{st}}_{00}$ term in the expression (9) of the static potential. Applying $v^{A_1,\mathrm{st}}_{00}$ in the present calculation, we obtained the same DDCS results as presented in [23]. As further check of the code and the numerical methods, we evaluated DDCSs for the single ionization of H_2 induced by 95 keV H^+ and 1 MeV/amu C^{6+} projectiles, and close agreement was found with results reported in [22].

III. RESULTS AND DISCUSSIONS

The above generalization of the CDW-EIS model is applied to study the angular and energy distribution of electrons ejected under the impact of H_2O by energetic bare projectiles. As mentioned above, our interest is primarily focused on the ejection of low-energy electrons whose emission properties are very sensitive to the quality of the potential modeling the interaction of the released electron with the nuclei and the passive electrons. Three types of the e^--H_2O^+ interaction are taken into account in the evaluation of the continuum orbital of Eq. (10): (i) both static and exchange interactions are considered, (ii) only the multicenter static potential is included, (iii) only the spherically averaged static potential governs the ionized electron in the residual field of the target as in the case of the previous application of the CDW-EIS method to molecules [23]. Hereafter, these potentials are referred to as

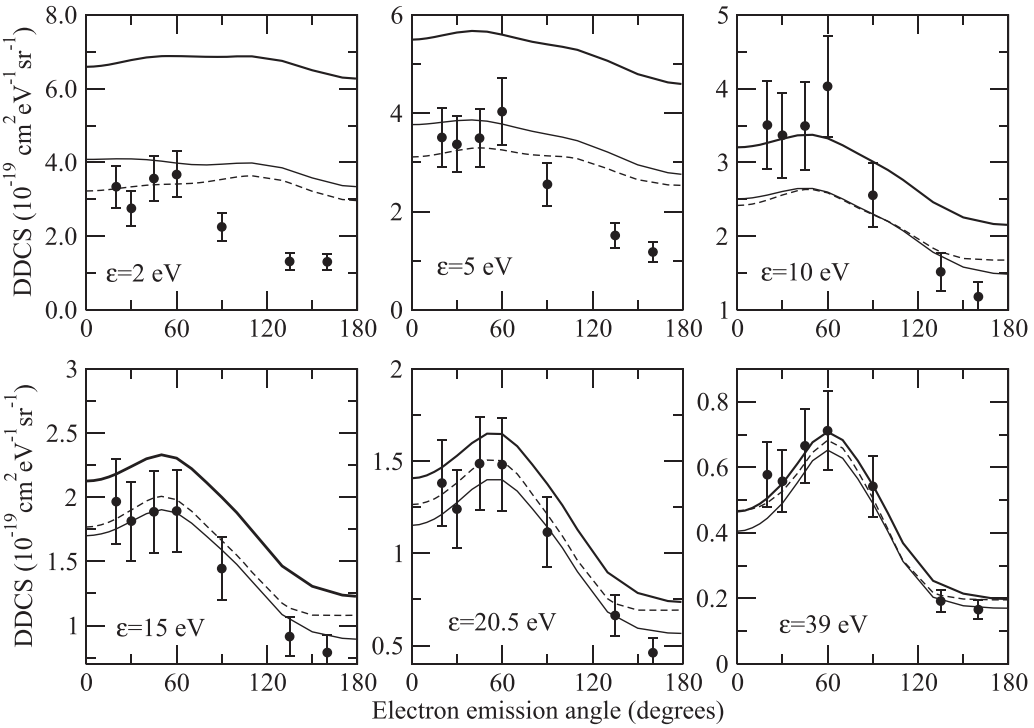

FIG. 1. DDCS for single ionization as a function of the electron emission angle for different electron energies for the 1 MeV H^+ projectile impact. Present CDW-EIS results are shown as heavy solid line, solid line, and dashed line, obtained with static-exchange, static, and spherical static potentials, respectively. The experimental data are shown as symbols [45].

static-exchange, static, and spherical static potentials, respectively.

A. Doubly differential cross sections

1. Proton impact

In Figure 1 DDCS results for the 1 MeV $H^+ + H_2O$ collision system are presented as a function of the electron emission angle θ_k for fixed values of ejection energies ϵ, where the present prior CDW-EIS results are confronted with the experimental results [45]. Considerable discrepancies can be observed between results obtained with the different H_2O^+ model potentials, especially at the lowest electron ejection energies. DDCSs derived with static and spherical static potentials are close to each other for all the studied electron ejection energies. The differences between them fall within the range of experimental errors; however, they give realistic description of the mechanism only at $\epsilon \geqslant 15$ eV. For the lower electron energies the agreement with the measurement is limited to forward or backward emission angles. Electron emissions in the forward direction are described properly for $\epsilon = 2$ and 5 eV, while for $\epsilon = 10$ eV better results are provided at backward angles. Calculations involving exchange interactions overestimate the measured data at low electron energies, which is particularly significant below 5 eV. Unlike the other two model calculations, calculation with the static-exchange potential gives a good account of the experiment for $\epsilon =$ 10 eV in the forward direction. The best agreement with the measured data, taking into account the other two calculations, is reported at $\epsilon = 39$ eV and at higher electron energies (not presented in the figure).

In Figure 2 angular distributions of the DDCS are shown for three electron energies in the case of 250 keV proton impact. The present calculated results are compared to the recent experimental data of Bhogale *et al.* [31] and to the other theoretical results obtained in the prior form of the CDW-EIS [9] and in the classical-trajectory Monte Carlo (CTMC) [46] approximations. As for the case of 1 MeV impact energy the present calculations with static-exchange potential slightly overestimate the measured data, and better agreements are reported when only the static potentials are included in the calculations. As in Fig. 1, the differences are minor between values of the DDCS derived with spherical and nonspherical static potentials. The CDW-EIS model reported in [31] overestimates the measured DDCS values at the forward and medium emission angles for all the studied electron energies. Let us first consider the results at $\epsilon = 3$ eV, where the largest discrepancy can be observed between the theories, and where the CTMC of [46] reveals a relatively good agreement with the measurement. Different predictions about the slope of DDCS distributions can be observed between the present and the other theoretical results. At low ϵ, the classical picture loses its validity as the dipole mechanism governs the process and the momentum transferred to the electron is small [47]. The slow electron spends a relatively long time in the field of the residual H_2O^+ ion in order for its movement to be significantly affected by the anisotropic character of the potential, which is also manifested in the shape of the angular distribution. It is also worth drawing attention to the significant differences in magnitude between results of the present prior CDW-EIS calculation obtained on the spherically static potential and of the prior CDW-EIS one presented in [31]. In the

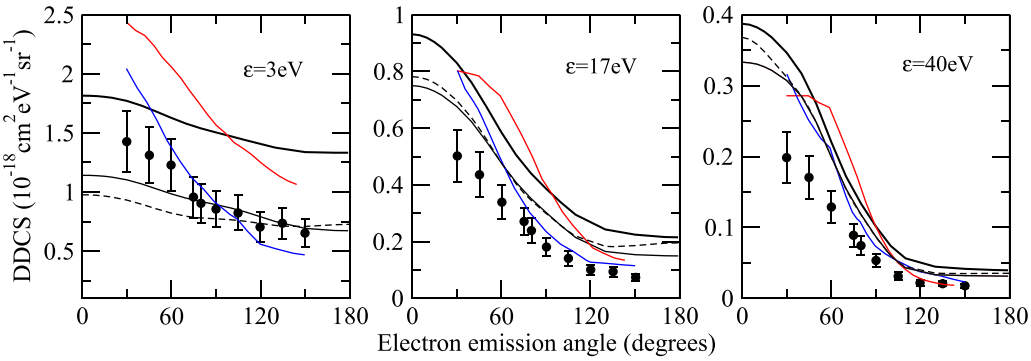

FIG. 2. DDCS for single ionization as a function of the electron emission angle for different electron energies for the 250 keV H^+ projectile impact. Present CDW-EIS results are shown as heavy solid line, solid line, and dashed line, obtained with static-exchange, static, and spherical static potentials respectively. Symbols are the experimental data, while red and blue lines are the theoretical prior CDW-EIS and CTMC results, respectively, all taken from [31].

applications of the CDW-EIS methods by Bhogale *et al.* [31], the initial orbitals were described by the complete neglect of differential orbitals (CNDO) approximation and the electron in the continuum was represented by the Coulomb potential with effective charge [9]. Both the CNDO and the effective Coulomb potential approximations neglect the multicenter nature of the ionization process, and together are responsible for the observed discrepancies between the present and earlier [31] applications of the CDW-EIS method. At higher electron energies, the shapes of the DDCS distributions are very similar in the different calculations, the trend of which matches the experiment. At $\epsilon = 40$ eV, discrepancies between the theories are in the range of experimental errors; however, all of them highly overestimate the measurement at the extreme forward emission angles.

2. O^{8+} *and* C^{6+} *impacts*

In Fig. 3 theoretical and experimental DDCS results for the ionization of water by impact of 4.5 MeV/amu O^{8+} ions are shown as a function of the electron emission angle at some electron emission energies. Pronounced peaks dominating the angular distributions at $\theta_k \approx 60^\circ$ can be observed in the measured data at the lowest electron emissions energies [48]. At the same time the present theoretical model calculations, as for the proton projectile (Sec. III A 1), predict a rather flat angular distribution. Results obtained with the static-exchange model potential are in agreement with the measured data within the limits of experimental errors in the region of medium ejection angles when $\epsilon \leqslant 11$ eV, while the other two model calculations show acceptable results only at the backward electron emission angles. For $\epsilon > 11$ eV, calculations based on the spherical potentials show almost the same results and all the present model calculations give similar account of the binary peak at $\epsilon = 40$ eV.

Other theoretical results, available for $\epsilon = 20$ and 40 eV, in both prior and post forms of the CDW-EIS approximation [9] and in the three Coulomb wave (3CW) model [20] are also shown in Fig. 3. In all of these calculations the bound state molecular orbitals have been represented in terms of Slater-type wave function centered on the the oxygen atom as proposed by Moccia [49]. Note the single center wave functions of Moccia [49] give a precise description of a multicenter orbital simialr to the ones presented in Eq. (7) for the case of XH_n type molecules [50]. However, in the description of the final channel the multicenter character of the molecule has been neglected, as the ejected electron in the field of the H_2O^+ ion has been represented by Coulomb wave function with an effective nuclear charge; see [9,20]. It is seen that the prior version of the CDW-EIS model describes properly the DDCS in the binary region, while the post form presents lower DDCS values at $\theta_k \approx 60^\circ$. The observed post-prior discrepancies between the two CDW-EIS results of [9] can be attributed to the fact that in the prior version the influence of the passive electrons on the dynamical evolution of the ejected electron is implicitly included, whereas in the post version it is only partially taken into account [9]. The results of the 3CW model show a nice agreement with the experiment in the whole angular region. As mentioned above, the interactions of the active electron with the target core, in both the initial and final channels, is considered similarly in the CDW-EIS [9,48] and in the 3CW [20] models. Therefore, the slopes of the DDCS distributions at the forward and backward emission angles predicted differently by the CDW-EIS and the 3CW calculations are mostly related to the intrinsic feature of the collision dynamics considered in various ways in these applications.

The DDCS data discussed so far show that the description of the electron ejection mechanism at electron energies below 10–15 eV poses serious challenges for the theories. Variations in the results of different model calculations often exceed the experimental error limits, and their performance varies for different collision systems. The perturbation strengths of the projectile, Z_p/v, are 0.15. 0.35, and 0.59, respectively for the 1 MeV H^+, 250 keV H^+, and 4.5 MeV/amu O^{8+} projectile ions. The CDW-EIS model is the first order of a distorted wave series in which the initial and final distorted waves are proposed by Eqs. (16) and (17), respectively [11]. Consequently, the best performance of the model is expected at lowest perturbation strength, which has not been fully confirmed by the discussions so far. Of course, there may also appear problems with the absolute and relative normalizations of experimental data, as noted in [46]. To verify the above

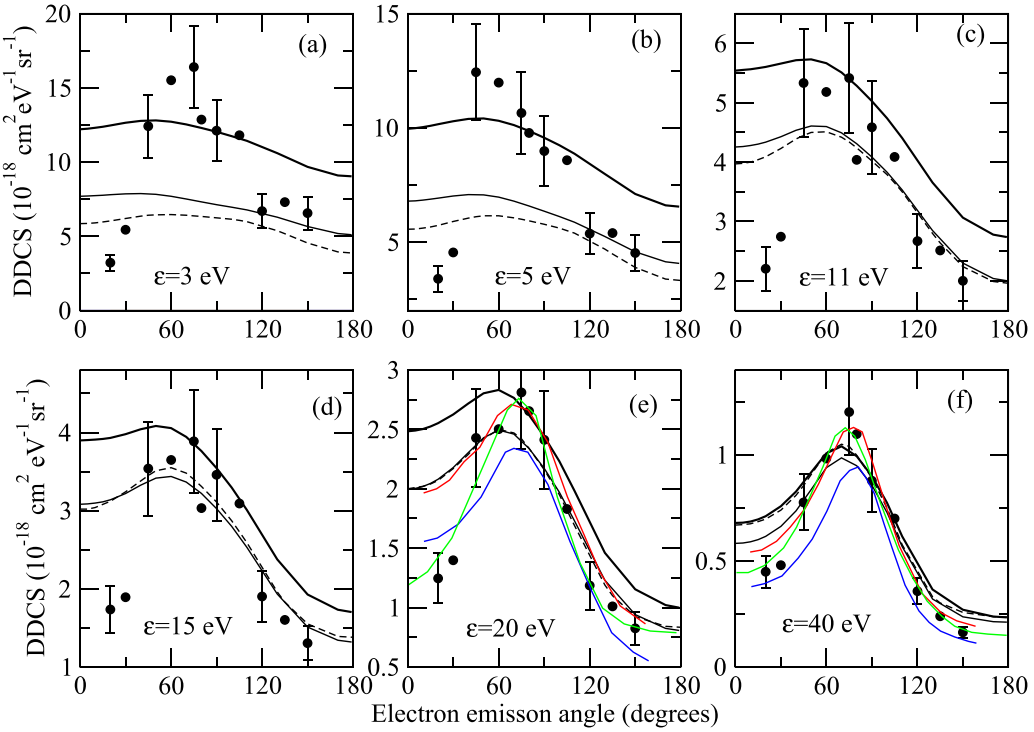

FIG. 3. DDCS for single ionization as a function of the electron emission angle for different electron energies for the 4.5 MeV/amu O^{8+} projectile impact. Present CDW-EIS results are shown as heavy solid line, solid line, and dashed line, obtained with static-exchange, static, and spherical static potentials respectively. Symbols are experimental data from [48]. Solid red and blue lines are the prior and the post CDW-EIS results, respectively [9]. The solid green line shows the 3CW result [20].

statements and explore more details on the validity of the model, we are extending the analysis of the DDCS to the following two collision systems.

Figure 4 presents the DDCS results for 6 MeV/amu C^{6+} and 3 MeV/amu O^{8+} projectiles having $Z_p/v = 0.38$ and 0.73 values, respectively. For the weaker perturbation (C^{6+} projectile), as for the case of the 1 MeV H^+ projectile (see Fig. 1), the present results including the static-exchange interaction potential overestimate the experimental data [21] at low ϵ values. Results of the CDW-EIS calculation of Tachino *et al.* [9] and of the 3CW model by Mondal *et al.* [20] are also presented for $\epsilon = 19.2$ eV. It is interesting to note that the prior CDW-EIS not only underestimates the measurement, but shows significantly smaller DDCS values than the present one obtained with spherically static potential, which is primarily due to the different representation of electrons ejected into the continuum with Coulomb and screened-Coulomb potentials, respectively. Shapes of the angular distributions are very similar in all model calculation, and discrepancies between them appear mostly on the absolute scale (see the graph for $\epsilon =$ 19.2 eV). Present calculations with static potentials and the post CDW-EIS of [9] give the best account of the measured data points in the peak region. However, it should be mentioned that all the calculated results are within the range of the large experimental errors bars. For the other $\epsilon = 9.6$ and 38.5 eV values, similar to $\epsilon = 19.2$ eV, present calculations with spherical or nonspherical static potentials show the best agreement with the measured data.

For the 3 MeV/amu O^{8+} projectile impact (lower graphs in Fig. 4) the CDW-EIS results from [51] are available for comparison for all the presented $\epsilon = 5$, 15, and 40 eV ejections energies. The present calculations with spherical and nonspherical static potentials underestimate the measured data for $\epsilon = 5$ eV. The trend is opposite when the exchange contribution to the active electron target core interaction is also included in the description. The CDW-EIS results of [51] in both prior and post forms show good agreement with the measurements. The CTMC results from [46] are also available for comparison, which shows the correct angular shape but the magnitude is underestimated. At $\epsilon = 15$ eV the present calculation including the static-exchange potential also overestimates the measurement, and predicts the nearly constant DDCS values in the forward direction. This prediction, which is also observed in the case static potentials, is in disagreement with the measurement and also not consistent with the prediction of the CDW-EIS calculation from [51]. A slight overestimation of the measurement in the present calculations at the forward emission angles can also be observed at $\epsilon =$ 40 eV. At this ejection energy the calculation with nonspherical static potential shows good agreement with the measured DDCS data. The CDW-EIS model [51] in the prior version predicts higher DDCS values than in the post form at all ϵ values. In the case of $\epsilon = 40$ eV the former application gives the best picture of the measurement, while for $\epsilon = 15$ eV the latter is best..

A comparison of the present DDCS results with results of the previous CDW-EIS applications (see Figs. 2–4) sheds light on the effect of the multicenter nature of the molecule in the studied processes. As noted above, the wave functions of Moccia [49], used by Tachio *et al.* [9] in their CDW-EIS

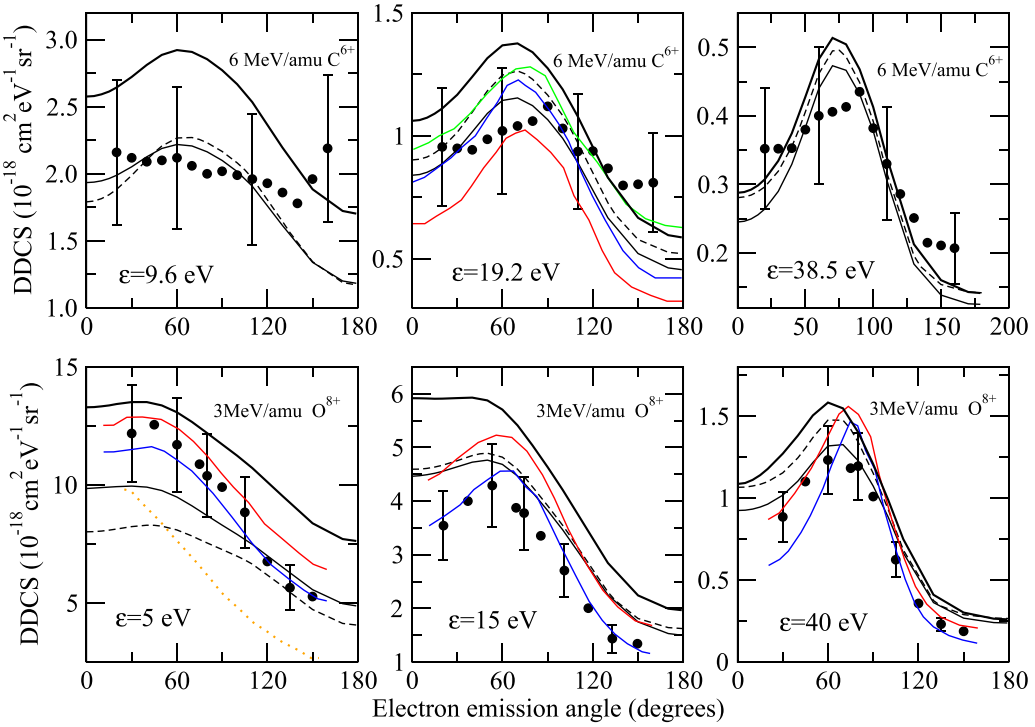

FIG. 4. DDCS for single ionization as a function of the emission emission angle for different electron energies. Present CDW-EIS results are shown as heavy solid line, solid line, and dashed line, obtained with static-exchange, static, and spherical static potentials, respectively. Symbols are experimental data from [21] for C^{6+} and [51] for O^{8+} impacts. Solid red and blue lines are the prior and the post CDW-EIS results for C^{6+} [9] and for O^{8+} [51] ions, respectively. The green line (C^{6+}, $\epsilon = 19.2$ eV) shows the 3CW data [20]; the dotted line (O^{8+}, $\epsilon = 5$ eV) is the CTMC data from [46].

descriptions, give a description of the bound state orbitals similar to the present SCE ones of Eq. (7). Therefore, the observed discrepancies between the DDCS results are mostly due the differences in the description of continuum sates. It is also clear from the figures that the choice of the potential is primarily important in the case of low-energy electrons. At higher electron energies the role of the active electron target-core interaction can be well described by an average field, represented by a Coulomb potential with properly chosen effective charge. Inclusion of the exchange interaction has a considerable effect on the evaluated DDCS. Taking into account this interaction always increases the values of DDCS, which leads to overestimation of the measured data in several cases. It should be noted, however, that the large experimental errors and inaccuracies in the data do not allow us to make more precise statements on the ability of theories. Note also that in all of the discussed calculations the initial and final wave functions for the active electron around the target core are not orthogonal, which might also have significant effect on the calculations and so on the conclusions [12].

Figure 5 displays the DDCS as a function electron energies for various emission angles for the 4.5 MeV/amu O^{8+} projectile. As can be expected from the study of angular distributions (see Fig. 3), the largest discrepancies between the calculations, using different H_2O^+ model potentials, appear at electron ejection energies lower than 40–50 eV. Differences between results derived with the spherical static and the static potentials are not visible in the graphs, therefore, results only of the later one are presented in the figure. At $\epsilon \geqslant 50$ eV all the calculations provide similar DDCS values. The prior CDW-EIS results of Nandi *et al.* [48] give a realistic description of the ejection mechanism for all emission angles. The present calculation with static potential underestimates the measurement at the medium emission angles when $\epsilon \leqslant 20$ eV, and good agreement is found in the case of the static-exchange model interaction potential. In the region of forward and backward emission angles the performance of these two model applications depends on θ_k.

B. Singly differential cross sections

In Fig. 6 SDCSs as a function of emission angle are shown for the 4.5 and 3 MeV/amu O^{8+} projectiles. Although the shapes of the evaluated SDCS distributions are similar to those of the measured distributions, significant quantitative differences can be observed between them for both projectile ions. Present calculations predict similar shapes for the SDCS with static and static-exchange interactions; however, differences between them on the absolute scale exceed the error limits of the experimental points in certain angular ranges. Calculations with static-exchange interaction show the closest agreement with the measurement for the case of 4.5 MeV/amu impact energy, while for the 3 MeV/amu projectile energy the treatment that considers only the static interaction reproduces better the experimental distribution. The post version of the CDW-EIS model describes the experimental distribution quite well for the 3 MeV/amu impact, whereas the prior version overestimates the data. The situation is not so clear in the

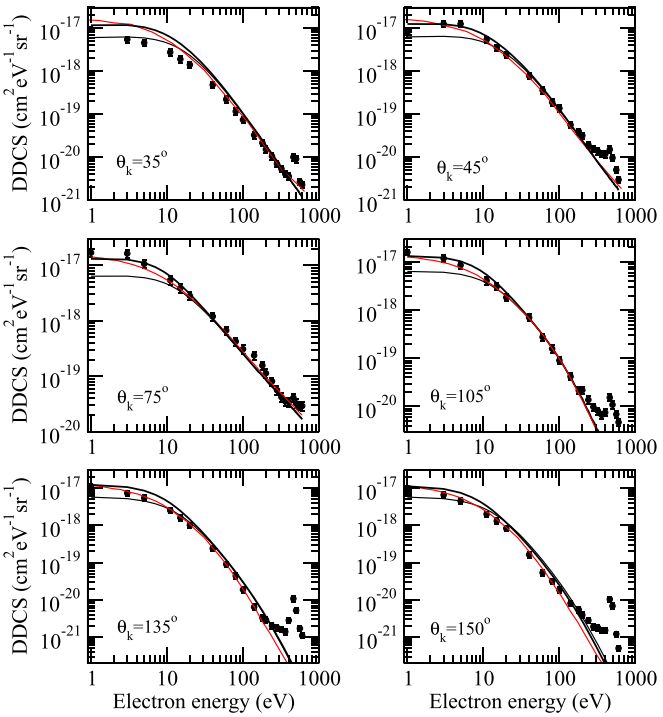

FIG. 5. DDCS for single ionization as a function of electron ejection energy for different emission angles for the 4.5 MeV/amu O^{8+} projectile impact. Present CDW-EIS results are shown as heavy solid line and solid line, obtained with static-exchange and static potentials, respectively. Symbols and the solid red lines show the experimental and the prior CDW-EIS results, respectively, from [48].

case of 4.5 MeV/amu collision energy, where result of the prior form shows a better agreement in the range of medium angular emission. Similarly, as we found in the analysis of DDCS data, the discrepancies between the present calculation with static potential and the prior CDW-EIS [48,51] highlights also the different treatments of the e^--H_2O^+ interaction in the exit channel. The CTMC result from [46], presented for the 3 MeV/amu impact energy, underestimates the measurement at the medium and backward emission angles. However, it

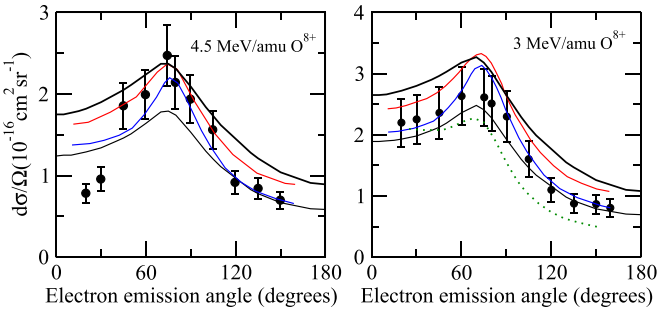

FIG. 6. SDCS for ionization as a function electron emission angle. The present CDW-EIS results are shown as heavy solid line and solid line, obtained with static-exchange and static potentials, respectively. Symbols are experimental data [48,51] and the prior and post CDW-EIS results are given by solid red and blue lines [48], respectively. The dotted line is the CTMC results from [46].

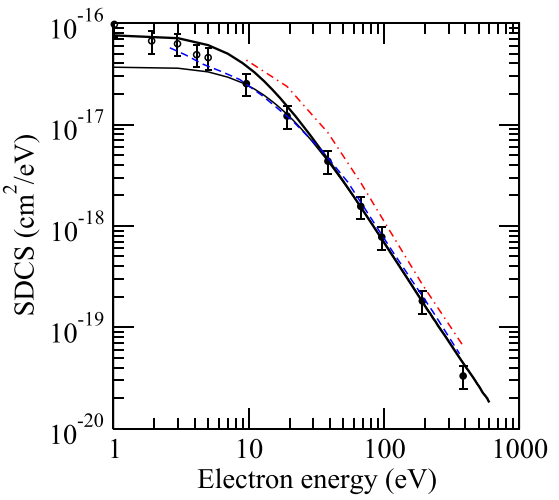

FIG. 7. Energy distribution of SDCS for the 6 MeV/amu-C^{6+} + H_2O collisions. Theory: present CDW-EIS obtained with static-exchange potential (heavy solid line), static potential (solid line), FBA from [21] (dot-dashed line), and CTMC from [28] (dashed line). Experimental results are from [21] (full circle) and [52] (open circle).

should also be pointed out that relatively large experimental errors do not make measurements suitable for more accurate evaluation of the validity of the calculations.

Single differential cross sections as a function of electron ejection energy Eq. (28) are shown in Fig. 7 for the case of 6 MeV/amu C^{6+} on impact. Results of the present and other theoretical calculations are compared with experimental data by the group of Ohsawa [21,52]. Our calculation, which includes the exchange interaction between the active electron and the core electrons, is in agreement with the measurement, except in the the narrow range of electron ejection energies around $\epsilon = 10$ eV. The SDCS of (28) is dominated by electrons emitted in the medium angular range, and at $\epsilon \approx 10$ eV the present calculation, as expected from Fig. 4, overestimates the measured data. However, the good agreement with the measurement at the lowest ejections energies indicates the non-negligible role of the exchange interaction in the process. This is more obvious if one considers that the calculation incorporates only the static part of the e^--H_2O^+ potential that presents a good account of the measurement only at $\epsilon \geqslant 10$ eV. The CTMC result of Jorge *et al.* [46] is in good agreement with the experimental data, while the first Born approximation (FBA) model [21] overestimates the measurement for all electron ejection energies.

Experimental and theoretical CDW-EIS total cross sections of Eq. (30) available for the considered collision systems are tabulated in Table I. The largest discrepancies between theories and experiments, which can even exceed 50%, can be observed in the case of the H^+ projectile ion. Present results with static-exchange interaction overestimate the measurement for all cases, while with static potentials, except for H^+, our calculations predict lower TCS values. It can also be stated that the differences in experimental and theoretical TCS data are largely due to differences in DDCS distributions at low electron energies. The fact that our calculations with static potentials in many cases underestimate experimental TCS

TABLE I. TCS values in 10^{-16} cm^2, for different projectiles. The other theories are the CDW-EIS applications presented together with the referred experimental data.

	Present results					
Projectile ion	Static exchange	Static	Sph. static	Other theory	Experiment	Ref.
250 keV H^+	3.2	2.61	2.57	2.99	1.62	[31]
6 MeV/amu C^{6+}	9.92	7.52	7.93	9.2	9.0	[28]
3 MeV/amu O^{8+}	3.08	2.13	2.20	2.8	2.33	[51]
4.5 MeV/amu O^{8+}	2.26	1.78	1.69	2.1	2.0	[48]

data suggests that contribution of exchange (or other, e.g., correlation) interaction should be included in the description. However, it seems that the currently used model results in an overestimation of the exchange contribution, which needs to be improved in the future development of the theory.

IV. SUMMARY AND CONCLUSIONS

In this paper we have presented an extension of the CDW-EIS model for computing differential and total cross sections for ionization of molecules by bare-ion impacts. Exceeding the limitations of previous applications [9,23], the wave function of the ionized electron has been evaluated on a more realistic, multicenter field of the residual target ion. In addition to the electrostatic interaction between the active electron and target core, contribution of the exchange interaction by a local energy-dependent potential has also been taken into account in the description. The initial multicenter molecular orbitals have been obtained at the Hartree-Fock level provided by the computer code GAUSSIAN16. The single-electron density on which the static and exchange potentials are derived has been determined on the ground state configuration of the molecule. The model has been tested for the case of ionization of the H_2O molecule by energetic proton and bare C and O projectiles.

A comparison of the DDCS and SDCS results evaluated on multicenter potentials with those in which the interaction of the ejected electron with the H_2O^+ ion was described on spherically symmetric Coulomb or screened Coulomb potentials, showed that the multicenter nature of the collision plays a determining role primarily in the ejection of low-energy electrons. It can also be concluded that the exchange potential plays a significant role in the ejection of low-energy electrons. For all the studied collision systems, inclusion of the exchange potential in the calculations increased the cross section values determined by static potential only. However, this fact does not always lead to a more accurate description of the measurement; see, e.g., the DDCS results presented in Figs. 1, 3, and 4. In many cases the discrepancies between results with static and static-exchange potentials exceed the error limits of the experiments. However, it should be mentioned that the applied local exchange potential is an approximation of the real one. It may also limit the performance of the present model that the initial and final one-electron orbitals are not orthogonal. A more accurate consideration of exchange interaction is one of our future plans in the development. However, other factors, such as the breakdown of the independent particle picture, etc, might also modify the performance of the theory. As mentioned in the Introduction, the correlation-polarization potential might also play an important role in the low-energy electron emission. Different methods are available to model the correlation-polarization interaction, and to test the role of this interaction we have applied the locale correlation-polarization model potential based on the density-functional theory [53,54] in our calculation. Calculations for the 1 MeV H^+ projectile have shown that the DDCS values evaluated at $\epsilon = 2$ eV varied by less than 10% as compared to the data shown in Fig. 1, which were obtained only with the exchange potential.

The present results show that describing emission of the low-energy electrons in ionization of the water molecule by energetic bare projectiles poses a major challenge to the theories. Our model calculations on the studied collision systems have not provided a consistent picture of the role of the considered e^--H_2O^+ interactions. In some cases, the calculations performed only with static interaction revealed the best agreement with the measurements, while in other cases this proved to be insufficient. The nature of the interaction, symmetric or asymmetric, Coulomb or screened-Coulomb, has also revealed different pictures in the studied collision systems. Results of the other theoretical descriptions (three-center CTMC, single-center CDW-EIS, 3CW, and first Born; see Figs. 2–7) considered in the discussions, also suggest that no theoretical method is capable of providing an accurate description of the low-energy electron emission in energetic ion molecule collisions. At the same time, we cannot ignore the fact that measuring low-energy electrons is an extremely difficult task, as probably highlighted by the unrealistic irregularities observed in the DDCS angular distributions; see, e.g., Figs. 1 and 3.

The great advantage of the present method is that it can be easily extended to discuss other molecules as well. The orbitals of the active electron both in the initial and final channel are treated by the SCE procedure. The symmetry of the molecule is taken into account in the evaluation of transition amplitudes, which reduces tremendously the time of computing.

ACKNOWLEDGMENTS

This work was supported by the Hungarian Scientific Research Fund (Grant No. K128621). The author wish to thank Prof. A Salin (University of Bordeaux) for discussion on the evaluation of coupled-channels equations.

[1] N. Stolterfoht, R. D. DuBois, and R. D. Rivarola, *Electron Emission in Heavy Ion-Atom Collisions* (Springer, Berlin, 1997).

[2] *Advances in Quantum Chemistry*, Vol. 65, edited by D. Belkic (Elsevier, Amsterdam, 2013).

[3] D. Belkić, I. Bray, and A. Kadyrov, State-of-the-art Reviews on Energetic Ion-atom and Ion-molecule Collisions, *Interdisciplinary Research On Particle Collisions And Quantitative Spectroscopy*, Vol. 2 (World Scientific Publishing Company, Singapore, 2019).

[4] A. M. P. Mendez, C. C. Montanari, and J. E. Miraglia, J. Phys. B: At., Mol. Opt. Phys. **53**, 175202 (2020).

[5] J. Ullrich, R. Moshammer, A. Dorn, R. Dörner, L. P. H. Schmidt, and H. Schmidt-Böcking, Rep. Prog. Phys. **66**, 1463 (2003).

[6] H. J. Lüdde, T. Spranger, M. Horbatsch, and T. Kirchner, Phys. Rev. A **80**, 060702(R) (2009).

[7] C. Illescas, L. F. Errea, L. Méndez, B. Pons, I. Rabadán, and A. Riera, Phys. Rev. A **83**, 052704 (2011).

[8] C. Champion, M. Galassi, P. Weck, O. Fojón, J. Hanssen, and R. Rivarola, in *Radiation Damage in Biomolecular Systems*, edited by G. García Gómez-Tejedor and M. C. Fuss (Springer, Dordrecht, 2012), pp. 263–289.

[9] C. A. Tachino, J. M. Monti, O. A. Fojón, C. Champion, and R. D. Rivarola, J. Phys. B: At., Mol. Opt. Phys. **47**, 035203 (2014).

[10] E. F. van Dishoeck, Faraday Discuss. **168**, 9 (2014).

[11] D. S. F. Crothers and L. J. Dube, in *Advances in Atomic, Molecular, and Optical Physics*, Vol. 30, edited by D. Bates and B. Bederson (Elsevier, Amsterdam, 1992), p. 287.

[12] L. Gulyás, P. D. Fainstein, and A. Salin, J. Phys. B: At. Mol. Opt. Phys. **28**, 245 (1995).

[13] M. R. Fiori, G. Jalbert, C. E. Bielschowsky, and W. Cravero, Phys. Rev. A **64**, 012705 (2001).

[14] M. J. Frisch *et al.*, *Gaussian 09 Revision A.1,* Gaussian Inc., Wallingford CT, 2009.

[15] B. H. Bransden and C. J. Joachaim, *Physics of Atoms and Molecules* (John Wiley and Sons, New York, 1987).

[16] F. A. Gianturco, D. G. Thompson, and A. K. Jain, in *Computational Methods for Electron Molecule Collisions*, edited by W. M. Huo and F. A. Gianturco (Plenum, New York, 1994).

[17] F. A. Gianturco and A. Jain, Phys. Rep. **143**, 347 (1986).

[18] M. E. Galassi, R. D. Rivarola, M. Beuve, G. H. Olivera, and P. D. Fainstein, Phys. Rev. A **62**, 022701 (2000).

[19] M. E. Galassi, R. D. Rivarola, and P. D. Fainstein, Phys. Rev. A **70**, 032721 (2004).

[20] A. Mondal, C. R. Mandal, and M. Purkait, J. Phys. B: At., Mol. Opt. Phys. **49**, 075201 (2016).

[21] C. Dal Cappello, C. Champion, O. Boudrioua, H. Lekadir, Y. Sato, and D. Ohsawa, Nucl. Instrum. Methods Phys. Res., Sect. B **267**, 781 (2009).

[22] R. F. Nascimento, L. E. Machado, C. E. Bielschowsky, and G. Jalbert, J. Phys. B: At. Mol. Opt. Phys. **41**, 225201 (2008).

[23] L. Gulyás, S. Egri, H. Ghavaminia, and A. Igarashi, Phys. Rev. A **93**, 032704 (2016).

[24] M. E. Riley and D. G. Truhlar, J. Chem. Phys. **65**, 792 (1976).

[25] S. Hara, J. Phys. Soc. Jpn. **22**, 710 (1967).

[26] U. Amaldi and G. Kraft, Rep. Prog. Phys. **68**, 1861 (2005).

[27] C. Champion, O. Boudrioua, and C. D. Cappello, J. Phys.: Conf. Ser. **101**, 012010 (2008).

[28] T. Liamsuwan and H. Nikjoo, Phys. Med. Biol. **58**, 641 (2013).

[29] P. de Vera, I. Abril, and R. Garcia-Molina, Radiat. Res. **190**, 282 (2018).

[30] L. Ábrók, T. Buhr, Ákos Kövér, R. Balog, D. Hatvani, P. Herczku, S. Kovács, and S. Ricz, Nucl. Instrum. Methods Phys. Res., Sect. B **369**, 24 (2016).

[31] A. Bhogale, S. Bhattacharjee, M. R. Chowdhury, C. Bagdia, M. F. Rojas, J. M. Monti, A. Jorge, M. Horbatsch, T. Kirchner, R. D. Rivarola *et al.*, Phys. Rev. A **105**, 062822 (2022).

[32] M. Gong, X. Li, S. B. Zhang, S. Niu, X. Ren, E. Wang, A. Dorn, and X. Chen, Phys. Rev. A **98**, 042710 (2018).

[33] S. B. Zhang, X. Y. Li, J. G. Wang, Y. Z. Qu, and X. Chen, Phys. Rev. A **89**, 052711 (2014).

[34] E. Acebal and S. Otranto, Phys. Rev. A **102**, 042808 (2020).

[35] B. H. Bransden and M. R. C. McDowell, *Charge Exchange and the Theory of Ion-atom Collisions* (Clarendon, Oxford, 1992).

[36] A. P. P. Natalense and R. R. Lucchese, J. Chem. Phys. **111**, 5344 (1999).

[37] S. L. Altmann and A. P. Cracknell, Rev. Mod. Phys. **37**, 19 (1965).

[38] R. G. Newton, *Scattering Theory of Waves and Particles* (Springer, New York, 1982).

[39] A. Igarashi, L. Gulyás, and P. Fainstein, Eur. Phys. J. D **42**, 73 (2007).

[40] A. R. Edmonds, *Angular Momentum in Quantum Mechanics* (Princeton University Press, Princeton, 1957).

[41] D. Dill and U. Fano, Phys. Rev. Lett. **29**, 1203 (1972).

[42] R. Hoffmann, J. Chem. Phys. **39**, 1397 (1963).

[43] G. Herzberg, *Molecular Spectra and Molecular Structure III. Electronic Spectra and Electronic Structure of Polyatomic Molecules* (Van Nostrad, Princeton, 1966).

[44] M. J. Frisch, G. W. Trucks, H. B. Schlegel, G. E. Scuseria, M. A. Robb, J. R. Cheeseman, G. Scalmani, V. Barone, G. A. Petersson, H. Nakatsuji *et al.*, *Gaussian 16 Revision C.01, Gaussian Inc.* (Wallingford, CT, 2016).

[45] S. T. S. Kovács, P. Herczku, Z. Juhász, L. Sarkadi, L. Gulyás, and B. Sulik, Phys. Rev. A **94**, 012704 (2016).

[46] A. Jorge, M. Horbatsch, C. Illescas, and T. Kirchner, Phys. Rev. A **99**, 062701 (2019).

[47] C. O. Reinhold and J. Burgdorfer, J. Phys. B: At. Mol. Opt. Phys. **26**, 3101 (1993).

[48] S. Nandi, S. Biswas, A. Khan, J. M. Monti, C. A. Tachino, R. D. Rivarola, D. Misra, and L. C. Tribedi, Phys. Rev. A **87**, 052710 (2013).

[49] M. Moccia, J. Chem. Phys. **40**, 2186 (1964).

[50] L. Gulyás, I. Tóth, and L. Nagy, J. Phys. B: At. Mol. Opt. Phys. **46**, 075201 (2013).

[51] S. Bhattacharjee, S. Biswas, C. Bagdia, M. Roychowdhury, S. Nandi, D. Misra, J. M. Monti, C. A. Tachino, R. D. Rivarola, C. Champion *et al.*, J. Phys. B: At. Mol. Opt. Phys. **49**, 065202 (2016).

[52] D. Ohsawa, Y. Hashimoto, S. Muto, T. Okada, H. Tawara, T. Honma, T. Murakami, and F. Soga, HIMAC-132 report, National Institute of Radiological Sciences, Chiba, Japan, 2009 (unpublished).

[53] F. A. Gianturco, A. Jain, and J. A. Rodriguez-Ruiz, Phys. Rev. A **48**, 4321 (1993).

[54] N. Sanna and F. Gianturco, Comput. Phys. Commun. **128**, 139 (2000).